DOI: 10.1111/mice.13050

INDUSTRIAL APPLICATION

COMPUTER-AIDED CIVIL AND INFRASTRUCTURE ENGINEERING WILEY

A vision monitoring system for multipoint deflection of large-span bridge based on camera networking

Yihe Yin[1,2] | Qifeng Yu[1,2] | Biao Hu[1,2] | Yueqiang Zhang[1,2] | Wenjun Chen[1,2] | Xiaolin Liu[1,2] | Xiaohua Ding[3]

[1]College of Physics and Optoelectronic Engineering, Shenzhen University, Shenzhen, China

[2]Institute of Intelligent Optical Measurement and Detection, Shenzhen University, Shenzhen, China

[3]Shenzhen Eagle Eye Online Electronic Technology Co. Ltd., Shenzhen, China

Correspondence
Xiaolin Liu, College of Physics and Optoelectronic Engineering, Shenzhen University, Shenzhen, 518060, China.
Email: liuxiaolinszu@163.com

Funding information
National Key Research and Development Program of China, Grant/Award Number: 2019YFC1511102; National Natural Science Foundation of China, Grant/Award Numbers: 12002215, 52208399; China Postdoctoral Science Foundation, Grant/Award Numbers: 2021M702266, 2022T150437

Abstract

This paper proposes a vision monitoring system for multipoint deflection of a large-span bridge that can well compensate the camera motion–induced errors. The camera network system (CNS) consists of a series of dual-camera stations that are linked with the cooperative markers. The infrared illumination supplement device is integrated in the camera station and the regular double-sided prism is selected as the cooperative marker to realize 24-h continuous monitoring. The feasibility and efficiency of CNS are verified by conducting a field test inside the steel box girders of a suspension bridge with a length of 1038 m. The results show that the proposed camera networking method can well solve the problem of the large-scale high-precision monitoring under unstable measuring platform. For the kilometer-level flexible bridge, CNS can meet submillimeter precision in quasi-static measurement, and can also provide deflection data similar to the conventional robotic total station and connecting pipe system in long-term monitoring. The geometric alignment of large-span bridges with dense multimeasuring points can be automatically monitored and recorded by CNS. The observed deflections of the studied suspension bridge are dominated with the vehicle load and wind load in the short term and are correlated with the temperature change in the long term. The proposed CNS can provide a new option for the bridge deflection monitoring and provide new parameters for bridge safety evaluation.

1 | INTRODUCTION

Bridge is one of the most important civil infrastructures in modern society. Under the effect of complex operating environment, the materials will inevitably age and damage, and the bearing capacity of the long-span bridges will decline. The accumulation of damage to a certain extent will affect the safety performance of the bridge (Feng & Feng, 2018; Li et al., 2006; Zhang et al., 2021). The structural control and health monitoring is an important research topic for bridge safety (Amezquita-Sanchez et al., 2018; Ghaedi et al., 2017; Sirca & Adeli, 2018). Several structural control methods and systems have been proposed to reduce the effect of dynamic load (e.g., traffic, wind, and earthquake) on a bridge (Adeli & Saleh, 1997; Gutierrez Soto & Adeli, 2019; Kim & Adeli, 2005). Meanwhile, large efforts have been devoted to the structural health monitoring, including but not limited to the defect detection

(Chun et al., 2022; Sajedi & Liang, 2021; Zhang & Lin, 2022; Zheng et al., 2022), stress or force estimation (Lee & Park, 2011; Tian et al., 2021), and strain or displacement measurement (Hampshire & Adeli, 2000; Park et al., 2007; Yu et al., 2022). As the most direct embodiment of structural health, the deflection of large-span bridge is an important index for the evaluation of bridge safety and applicability, which can be further used for the bridge properties identification (Amezquita-Sanchez & Adeli, 2019; Amezquita-Sanchez, Park, & Adeli, 2017; Perez-Ramirez et al., 2016; Pezeshki et al., 2023), structural response prediction (Perez-Ramirez et al., 2019; Ren et al., 2021), and early warning (Bao et al., 2019; Li et al., 2015; Oh et al., 2017; Sousa Tome et al., 2020).

Large efforts have been devoted to the deflection monitoring of large-span bridges, which can be categorized into nonautomatic and automatic methods. The nonautomatic monitoring method mainly refers to the leveling elevation method, such as total station, theodolite, and level. The leveling and elevation of a bridge are measured manually and regularly, which has the disadvantages of being time consuming and laborious, traffic interruption, poor real-time performance, and so forth. To satisfy the long-term operation needs, several mature automatic monitoring systems have been applied in the large-span bridges, including but not limited to the robotic total station (RTS;Dos Santos et al., 2019; Psimoulis & Stiros, 2013), global navigation satellite system (GNSS; Niu et al., 2021; Yi et al., 2013; Yu et al., 2014), and connecting pipe system (CPS; Liu et al., 2015; Zhou et al., 2021). RTS can be regarded as an automatic improvement of leveling and elevation method. It typically scans the bridge measuring points in turn according to the set procedure to get the deflection of the bridge. However, a single RTS cannot perform multipoint simultaneous monitoring. GNSS can directly obtain the three-dimensional (3D) absolute coordinates of the measuring point, while the accuracy of dynamic monitoring is low, generally in the order of centimeters. CPS can realize multipoint synchronous monitoring of bridge deflection, whereas has a poor dynamic performance.

With the development of digital image processing technology, computer vision (CV) method is gradually applied to the field of bridge engineering due to the advantages of nondestructive, noncontact, fast, and high precision (Dong & Catbas, 2021; Spencer et al., 2019; Stephen et al., 1993). Using the cameras as the displacement sensor, the deflection of the large-span bridge can be obtained by detecting and tracking the targets on the bridge (Lydon et al., 2019; Ngeljaratan et al., 2021; Park et al., 2015; Yu & Zhang, 2020). For example, Zhao et al. (2019) proposed a two-step combination of support correlation filter algorithm and Kanade–Lucas–Tomasi algorithm to identify the displacement of cable-stayed bridges from a video. Zhuge et al. (2022) carried out bridge deflection measurement based on a team of unmanned aerial vehicles (UAVs). Nasimi and Moreu (2021) proposed a system combining camera and laser to measure the total displacement of the structure. Shajihan et al. (2022) built a wireless SmartVision system for the multipoint displacement estimation. In addition to measuring one-dimensional displacement, visual-based measurement methods can also be used to measure 3D displacement. For example, Park et al. (2015) proposed a motion capture system based on the principle of multiple camera intersection measurement, which can measure the 3D displacement of a structure with a high accuracy and sampling rate. Zhao et al. (2022) measured 3D displacement of a structure based on monocular camera with known geometry.

Note, the aforementioned vision methods were performed based on the assumption that the camera is fixed in a strictly stable position, which is impractical for long-term monitoring (Shang et al., 2014; Yu et al., 2015). Several researchers tried to compensate the camera motion–induced errors in the long-term monitoring of bridge deflection (Lee et al., 2020; Pan et al., 2016; Yu et al., 2022). For example, Lee et al. (2020) proposed a dual-head camera system that can simultaneously measure and correct the ego motion of the observation platform. Yu et al. (2022) proposed a multicamera system composed of multiple correcting cameras and measuring cameras, which can accurately correct the influence of the platform 6-degree-of-freedom ego-motion on the measurement results. However, those methods are not suitable for the large-span bridge. It is known that the camera resolution decreases with the measurement distance. For large-span bridges, it is difficult to use a single camera to meet high measurement accuracy and simultaneous measurement of multiple points over a large span at the same time.

In view of large-scale subgrade settlement monitoring, the authors (Yu et al., 2015) have proposed displacement-relay videometrics method to realize settlement measurement on the unstable measuring platform. Further, the closed-loop camera series network was proposed for deformation measurement of large-scale structures (Yu et al., 2019), which is expected to realize deformation monitoring of the ring foundation pit. However, the above research only put forward the concept, and there are still many problems in the field application, which remain a further study. To this end, this paper proposes a vision monitoring system for multipoint deflection of a large-span bridge based on the principle of camera networking, denoted as camera network system (CNS). The system consists of a series of dual-camera stations

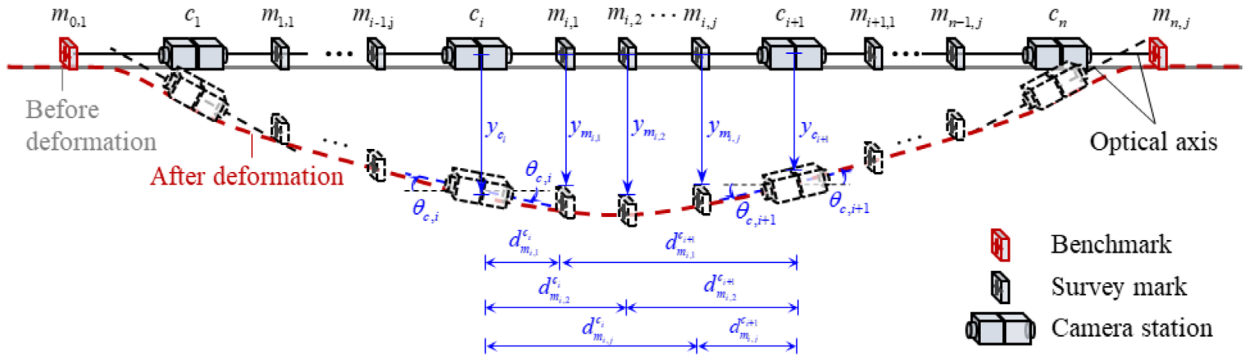

FIGURE 1 Schematic diagram of the proposed camera network system (CNS).

that are linked with the cooperative markers. CNS can well compensate the camera motion–induced errors and thus can be directly arranged on the unstable platform, such as bridge deck or steel box girder. First, aiming at the structural characteristics of long-span bridges, the optical measurement equation is derived. Second, the practical dual-camera station is designed, and the camera station is equipped with an infrared illumination supplement device, together with regular double-sided prismatic target, to achieve 24-h uninterrupted monitoring. The feasibility and efficiency of CNS are verified by conducting a field test on a suspension bridge with a length of 1038 m, CNS is placed inside the steel box girder. Finally, the observed full-span bridge deflection is presented and discussed.

2 | MONITORING SYSTEM OF BRIDGE DEFLECTION BASED ON CAMERA NETWORKING

2.1 | Measurement principle

In this study, the principle of the displacement-relay videometrics (Yu et al., 2015) is first introduced. As shown in Figure 1, camera stations and cooperative markers are arranged at intervals along the span direction of the bridge to be monitored. The camera station comprises two cameras that shoot in opposite directions and are held together rigidly. Therefore, the vertical displacement and pitch angle of the two cameras in the same station are the same (denoted as "fixation constraint" herein). Furthermore, there is a "homologous constraint" between images of the same marker captured by different cameras in adjacent camera stations, which means that the vertical displacement of the same marker in different images is identical.

Based on the proposed two basic constraints, the displacement-relay measurement equations can be determined. Figure 1 depicts the relevant positions of camera stations and cooperative markers before and after deformation. Multiple measuring points can be arranged between two camera stations. First, take the measuring point $m_{i,j}$ and the camera station c_i on the left side of the measuring point as an example, the vertical displacement of $m_{i,j}$ in the image captured by c_i ($h^{c_i}_{m_{i,j}}$) is mainly affected by three factors: (1) vertical displacement of $m_{i,j}$ ($y_{m_{i,j}}$), (2) vertical displacement of c_i (y_{c_i}), and (3) pitch angle variation of c_i (θ_{c_i}). The detailed relationship can be defined as follows:

$$h^{c_i}_{m_{i,j}} = k^{c_i}_{m_{i,j}} \left(y_{m_{i,j}} - y_{c_i} + d^{c_i}_{m_{i,j}} \cdot \sin\theta_{c_i} \right) \tag{1}$$

where $k^{c_i}_{m_{i,j}}$ is the scaling factor of $m_{i,j}$ in the image captured by c_i, $d^{c_i}_{m_{i,j}}$ is the distance between $m_{i,j}$ and c_i.

Similarly, take the measuring point $m_{i,j}$ and the camera station c_{i+1} on the right side of the measuring point as an example, the detailed relationship can be defined as follows:

$$h^{c_{i+!}}_{m_{i,j}} = k^{c_{i+1}}_{m_{i,j}} \left(y_{m_{i,j}} - y_{c_{i+!}} - d^{c_{i+1}}_{m_{i,j}} \cdot \sin\theta_{c_{i+1}} \right) \tag{2}$$

where $k^{c_{i+1}}_{m_{i,j}}$ is the scaling factor of $m_{i,j}$ in the image captured by c_{i+1}, $d^{c_{i+1}}_{m_{i,j}}$ is the distance between $m_{i,j}$ and c_{i+1}.

Therefore, for any measuring point between two adjacent camera stations, the measurement equation can be obtained according to Equations (1) and (2), respectively. Taking the cooperative markers between the two camera stations (c_i and c_{i+1}) as examples, the measurement equations can be established as follows:

$$\begin{bmatrix} -k_{m_{i,1}}^{c_i} & k_{m_{i,1}}^{c_i} d_{m_{i,1}}^{c_i} & k_{m_{i,1}}^{c_i} & 0 & \cdots & 0 & 0 & 0 \\ -k_{m_{i,2}}^{c_i} & k_{m_{i,2}}^{c_i} d_{m_{i,2}}^{c_i} & 0 & k_{m_{i,2}}^{c_i} & \cdots & 0 & 0 & 0 \\ \vdots & \vdots & \vdots & \vdots & \ddots & \vdots & \vdots & \vdots \\ -k_{m_{i,j}}^{c_i} & k_{m_{i,j}}^{c_i} d_{m_{i,j}}^{c_i} & 0 & 0 & \cdots & k_{m_{i,j}}^{c_i} & 0 & 0 \\ 0 & 0 & k_{m_{i,1}}^{c_{i+1}} & 0 & 0 & 0 & -k_{m_{i,1}}^{c_{i+1}} & k_{m_{i,1}}^{c_{i+1}} d_{m_{i,1}}^{c_{i+1}} \\ 0 & 0 & 0 & k_{m_{i,2}}^{c_{i+1}} & 0 & 0 & -k_{m_{i,2}}^{c_{i+1}} & k_{m_{i,2}}^{c_{i+1}} d_{m_{i,2}}^{c_{i+1}} \\ \vdots & \vdots & \vdots & \vdots & \ddots & \vdots & \vdots & \vdots \\ 0 & 0 & 0 & 0 & 0 & k_{m_{i,j}}^{c_{i+1}} & -k_{m_{i,j}}^{c_{i+1}} & k_{m_{i,j}}^{c_{i+1}} d_{m_{i,j}}^{c_{i+1}} \end{bmatrix} \begin{bmatrix} y_{c_i} \\ \sin\theta_{c_i} \\ y_{m_{i,1}} \\ y_{m_{i,2}} \\ \vdots \\ y_{m_{i,j}} \\ y_{c_{i+1}} \\ \sin\theta_{c_{i+1}} \end{bmatrix} = \begin{bmatrix} h_{m_{i,1}}^{c_i} \\ h_{m_{i,2}}^{c_i} \\ \vdots \\ h_{m_{i,j}}^{c_i} \\ h_{m_{i,1}}^{c_{i+1}} \\ h_{m_{i,2}}^{c_{i+1}} \\ \vdots \\ h_{m_{i,j}}^{c_{i+1}} \end{bmatrix} \tag{3}$$

where j is the number of cooperative markers between two adjacent camera stations.

As shown in Figure 1, when there are n camera stations that are separated by j markers, respectively, the following measurement equation can be obtained:

$$K^{(2jn)\times((n+1)j+2n)} \cdot Y^{((n+1)j+2n)\times 1} = H^{(2jn)\times 1} \tag{4}$$

where K is the measurement matrix, Y is the vector composed of the vertical displacement and pitch angle of each camera station along with the vertical displacement of each marker, and H is the vertical pixel coordinate displacement of each marker in the image.

2.2 | Measurement system

Based on the proposed principle, the measurement system (i.e., CNS) composed of dual-head camera stations and regular double-sided prisms is designed. As shown in Figure 2, the camera station is composed of two camera modules and one terminal. For each camera module, a 45° flat mirror is set below the camera lens to convert the vertically placed camera to the horizontal direction. In addition, an infrared illumination supplement device is added to fill light to the regular double-sided prism, which can ensure that the measurement system operates normally for 24 h without interference from visible light. The camera selected in this paper integrates an I/O general-purpose input/output (GPIO) interface, which can wake up the camera stations through hardware triggering to collect images synchronously. The camera station designed in this paper has a processor terminal integrated on it for edge computing. The processor terminal can call the image processing algorithm to process the image acquired by the camera station to obtain the pixel coordinates of the feature points in the image, and then transmit only the pixel coordinates to the main server for the solution of the measurement equation, avoiding the transmission of raw images with large data volume, thus guaranteeing the real time of the deflection calculation. Two communication networks, fiber optic or wireless LAN (local area network), can be used to link the camera stations. The camera station uses the prime lens, so the components in the camera station are fixed and no longer need to be adjusted after they are deployed in the field. The design can ensure

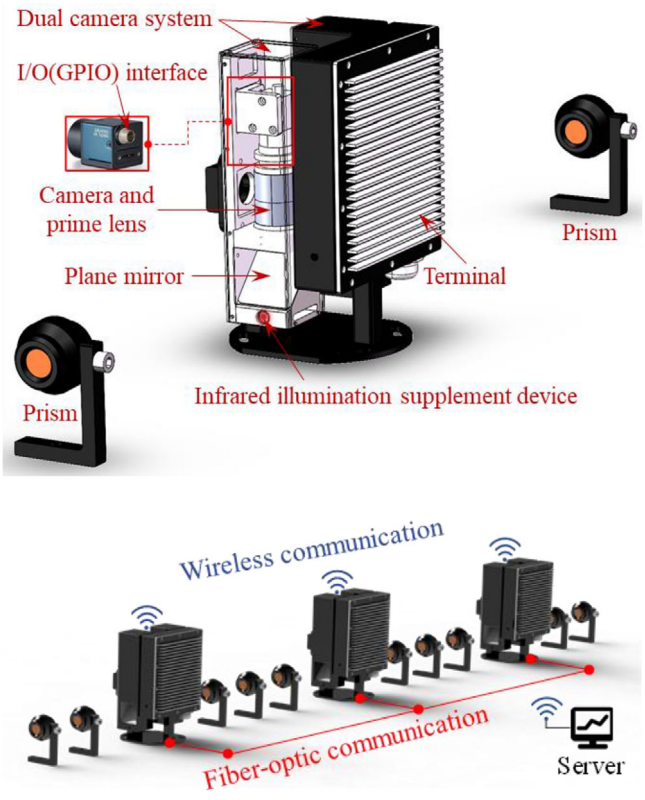

FIGURE 2 Camera network system (CNS) of bridge deflection monitoring.

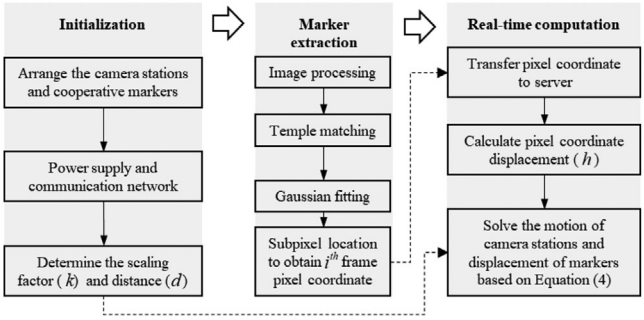

FIGURE 3 Measurement process of camera network system (CNS).

the fixation constraint and enhance the durability of the equipment. According to Figure 1, several camera stations are arranged along the structure to be monitored. It can be observed from Figure 2 that those stations are linked by regular double-sided prisms (i.e., cooperative markers), which is the "homologous constraint."

2.3 | Measurement process

Based on the proposed measurement principle and system, the multipoint deflection of the large-span bridge can be monitored. The detailed process is depicted in Figure 3. In the initialization stage, the camera stations and cooperative markers should be arranged first according to the design scheme. Note, the locations of camera stations and cooperative markers should be adjusted slightly to ensure that all the markers in the middle of the adjacent two camera stations can be captured in the images. Then, the power supply and communication network should be ensured. To establish the relationship between the pixels' coordinates (image) and the physical coordinates (structure), the scaling factor (k) of each marker should be determined by triangular geometric constraints (Feng et al., 2015). Also, the distances (d) between the camera stations and markers can be determined, respectively. Next, the marker extraction is conducted through the edge computing. Based on the synchronizing trigger signal, the images are captured synchronously for all the cameras. In each camera station, the feature of each marker is detected, tracked, and located, successively. In detail, the feature template of each cooperation markers is first determined. Then, the correlation coefficient matrix is obtained by template matching in the selected candidate region, and the extreme points are extracted by Gaussian fitting as the final subpixel location result (Wang et al., 2018). Finally, based on the built wired or wireless network, all the coordinate values of cooperation marks extracted in each station can be transferred to the server. The vertical displacement and pitch angle of each camera station, and the vertical displacement of each marker can be obtained simultaneously by solving Equation (4).

3 | FIELD TEST OF A SUSPENSION BRIDGE

3.1 | Test design

To validate the proposed measurement principle and system, a field test was carried out on a large-span suspension bridge. The studied bridge, called Qipanzhou Bridge, located in Hubei Province, China, is an important link of the Yangtze River for Wuhan city circle ring in the planning of the highway network. As shown in Figure 4a, the bridge investigated in this paper is a single-span 1038-m suspension bridge. It is noted that the test was conducted during the interval between the completion of the main bridge structure and the official opening to traffic. Thus, few vehicles passed the bridge except for those used for the construction of bridge ancillary structures. This provides a good test condition for the verification of the proposed CNS. Based on the proposed measurement principle and site situation, the measurement plan was conducted. As depicted in Figure 4b, the camera chain, consisting of 10 dual-head camera stations and 33 markers, is arranged symmetrically along the main span of the bridge. The camera stations next to the main tower (i.e., Stations 1 and 10) is 78 m away from the main tower, while other stations are arranged at an equal interval of 96 m. In addition, the markers at both ends are set at the main tower (i.e., benchmark), respectively. The detailed distance between each camera station and marker is shown in Figure 4b. The minimum scale factor of the proposed CNS in the field test is about 1.3 pixel/mm.

The proposed 10-station CNS was arranged inside the bilaterally symmetric steel box girder with a height of 3 m and a width of 38.5 m (Figure 4c). In detail, as shown in Figure 4d, the camera stations and prisms (i.e., cooperative markers) were set on the fence in the left inspection passage of the steel box girder. To ensure the quality of communication, fiber-optic communication is used in this field test to link the camera stations. The high-precision translation stage (Figure 4e,f) is used herein to provide a reference value of the displacement and pitch angle, which is used for the accuracy validation of the quasi-static measurement. Using the state of the bridge after CNS deployment is completed as the initial state for deflection measurements, following the process as shown in Figure 3, the all-span deflection can be observed with the established CNS.

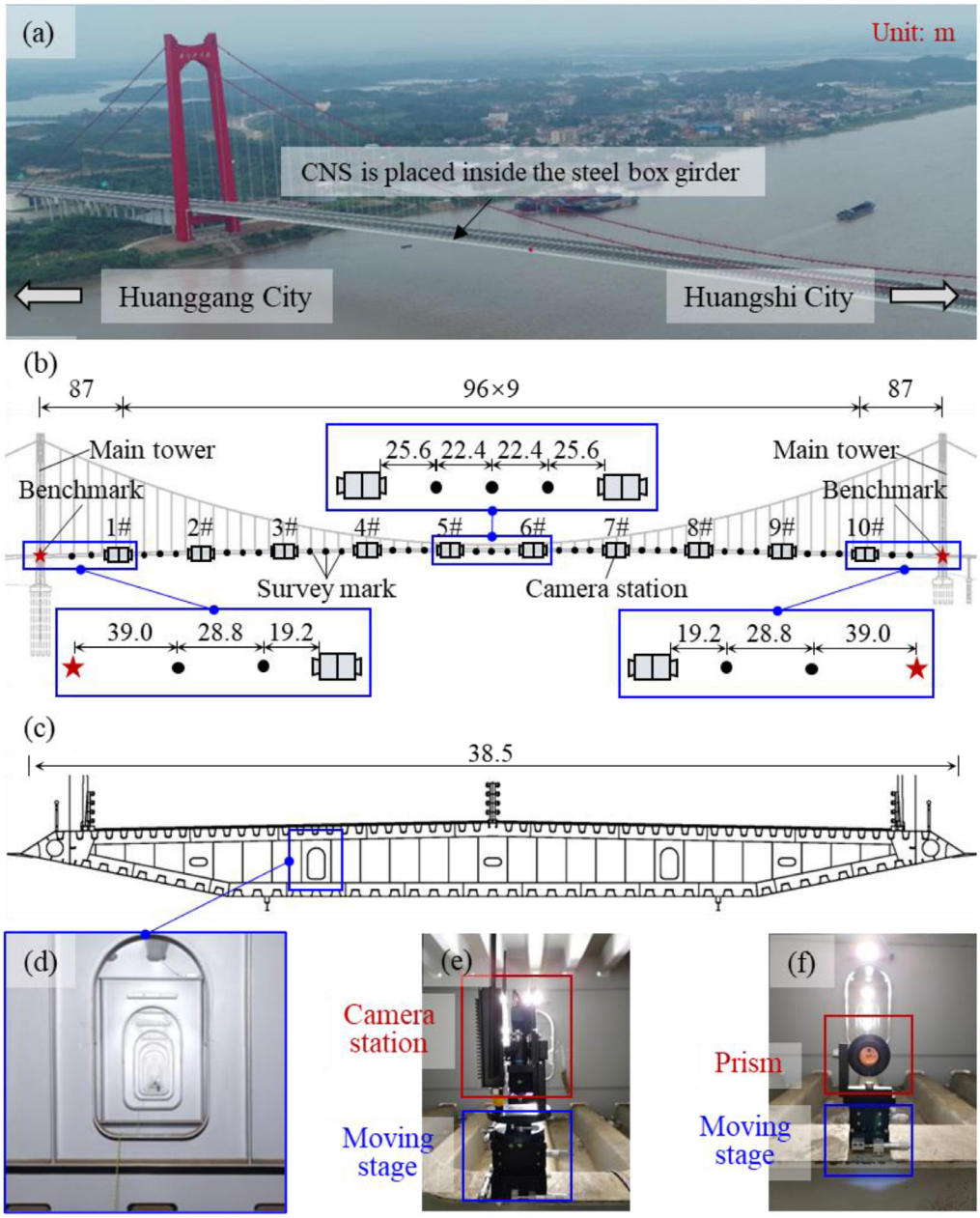

FIGURE 4 Field test: (a) actual view of the studied bridge; (b) schematic diagram of the proposed camera network system (CNS) field deployment; (c) cross-sectional diagram of main span steel box girder; (d) inspection passage of the steel box girder; (e) dual-camera station placed on a 5-axis moving stage; (f) prism marker placed on a two-dimensional moving stage.

3.2 | Quasi-static validation of CNS

The quasi-static validation test was first conducted on the 1038-m suspension bridge. It is known that the suspension bridge is a flexible structure whose vertical deflection is easy to change due to the external load, including but not limited to the vehicle load, wind load, and thermal load. Figure 5 shows the deflection response of the bridge main span for 28 h based on CNS. During the daytime, the passage of maintenance vehicles causes significant short-term fluctuations in the bridge deflection. However, during the night time, no fluctuation was induced by the vehicles due to the interruption of maintenance work. Therefore, the quasi-static verification experiment was chosen to be carried out between 1:30 a.m. and 1:40 a.m. The experimental process lasted about 10 min. No vehicle load was applied and the duration was short, and the effect of temperature change was negligible. Two types of quasi-static validation tests were conducted. The first test is to verify the accuracy of the proposed CNS when the camera station is not moved. The measuring points were artificially displaced with known true values, while the camera station was not artificially moved. The second test is to verify the motion compensation capability of

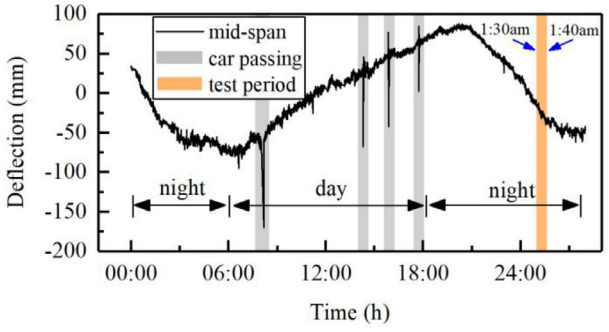

FIGURE 5 The deflection response of the bridge midspan for 28 h based on camera network system (CNS).

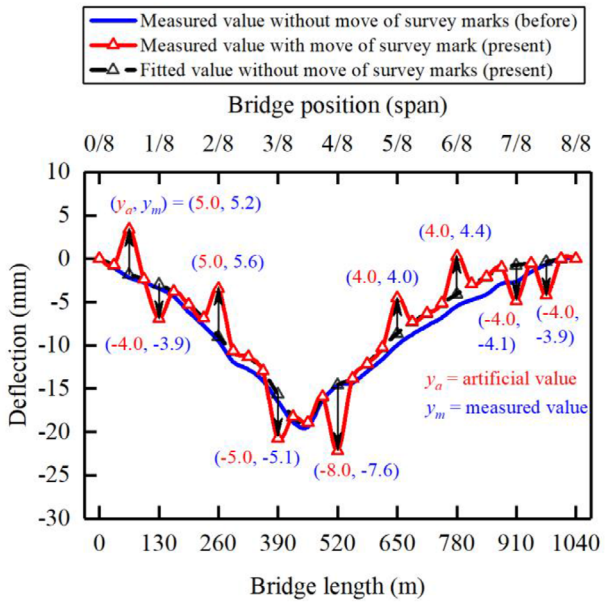

FIGURE 6 Schematic diagram of data processing and results for quasi-static validation.

CNS by artificial motion of both measuring points and camera stations. Note, the five-axis translation stage (Figure 4e) is used herein to provide the vertical displacement and pitch angle for the camera station, while the two-dimensional moving stage (Figure 4f) provides the vertical displacement for the markers.

Figure 6 depicts an example of the data processing and results for quasi-static verification. The artificial vertical displacements of nine different markers (denoted as reference points for quasi-static validation) along the bridge are provided by the two-dimensional moving stage. Based on the established CNS, the all-span bridge deflections before and after the move of those nine reference points can be obtained (see Figure 6). The convex or concave points can be observed at the position of those reference points. In addition, the deflection curve of the bridge also changed slightly during the quasi-static validation tests, which was mainly induced by the wind load.

TABLE 1 Quasi-static validation schemes.

Case	Camera station: Vertical displacement (mm)	Camera station: Pitch angle (′)	Cooperative marker vertical displacement (mm)
C1	0	0	−2
C2	0	0	−4
C3	2	0	0
C4	4	0	0
C5	−6	0	6
C6	0	−2.5	0
C7	0	1.5	−5
C8	0	−3	5
C9	2	3.5	0
C10	−4	−2.5	−6

In other words, the displacements of the aforementioned nine reference points consisted of the artificially generated displacements and the deflection changes due to external loads. To eliminate the influence of external-load–induced bridge deflection changes on the quasi-static validation tests, the deflection curve of the bridge in the current state was fitted from the measuring points without artificial displacement based on the continuity assumption of bridge deflection changes.

Based on the acquisition through a continuous frame of camera images, the measured deflection changes after the artificial move of the reference points were further obtained. Then, the measured values of the manually provided deflection change (y_m) can be obtained by subtracting the deflection fitted value from the deflection measured value. As shown in Figure 6, y_m values of those nine reference points are consistent with the artificial value (y_a). For example, the difference between y_m and y_a at the bridge position of 1/8, ¼, and 1/2 span are 0.1, 0.6, and 0.4 mm, respectively.

Following the data processing procedure as show in Figure 6, another 10 quasi-static validation cases were performed herein and the arrangement is listed in Table 1. Note, both the influence of vertical displacement and pitch angle of camera stations on the measurement results were considered. The measured deflection changes of the bridge at 1/4, ½, and 3/4 span are selected and compared with the artificial value (i.e., vertical displacement of corresponding cooperative markers in Table 1). As depicted in Figure 7a, the difference between the measured and artificial value in different cases is generally less than 1.0 mm. The proposed CNS can simultaneously measure the deflection change of the measuring point and the ego-motion of the camera station. Figure 7b shows the measured results of vertical displacement and pitch angle ego-motion of the 3# cam-

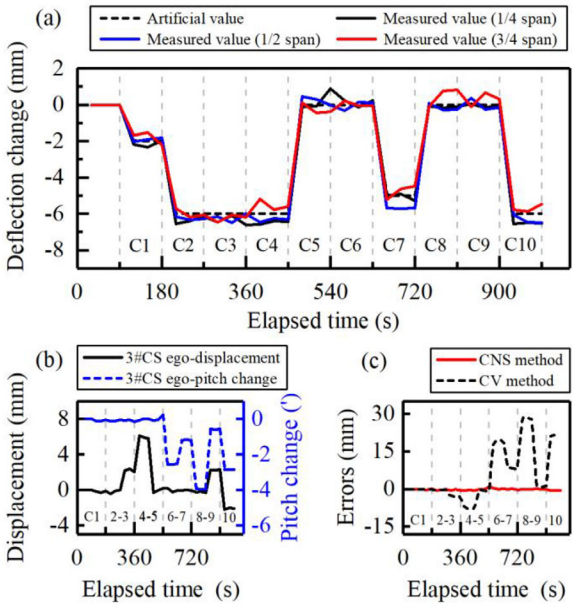

FIGURE 7 Validation results: (a) quasi-static validation results in different cases; (b) 3# camera station self-motion measured results; (c) comparison of the bridge deflection at 1/4 span observed based on camera network system (CNS) and traditional computer vision (CV).

TABLE 2 Quasi-static validation experiment measurement error statistics.

	1/4 span (mm)	1/2 span (mm)	3/4 span (mm)	3# camera station displacement (mm)	3# camera station pitch (′)
Max errors	.89	.90	.82	.35	.22
Root mean squared errors	.37	.39	.39	.20	.12

era station. The measurement errors were calculated and listed in Table 2.

Furthermore, the bridge deflection of 1/4 span obtained using CNS method and traditional CV method (i.e., camera without motion compensation; Chen et al., 2020) is compared herein. As shown in Figure 7c, the measurement errors of those two methods were consistent when there was no motion of camera station in the stage of Case 1 and Case 2. In subsequent Cases 3~5, the vertical displacements of camera station were artificially given. Larger measurement error of the CV method began to appear. Furthermore, the measurement error of the CV method becomes larger when the camera station has self-motion of pitch angle change (i.e., Cases 6~10). A small angle change can cause significant measurement error in the bridge deflection monitoring. On the contrary, the measurement results based on CNS can well compensate the measurement error caused by camera station

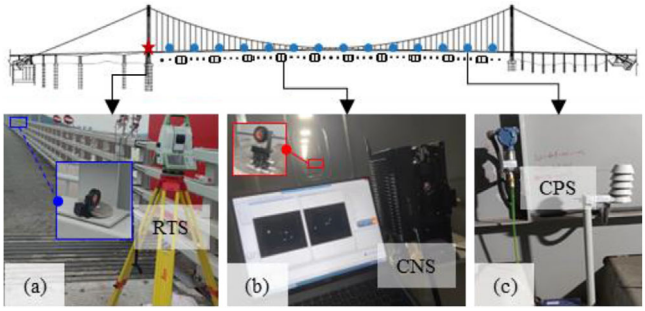

FIGURE 8 Measurement system of bridge deflection: (a) robotic total station (RTS); (b) camera network system (CNS); and (c) connected pipe system (CPS).

self-motion. The measurement errors can be controlled within 1.0 mm after the compensation. In summary, the proposed CNS method can effectively correct the effect of camera station self-motion on the measurement results, and is suitable for monitoring the deflection of flexible structures such as large-span suspension bridges.

3.3 | Long-term validation of CNS

The long-term monitoring of bridge deflection was further carried out. Figure 8 depicts the relationship between the RTS, connected pipe system (CPS), and the proposed CNS deployed on the bridge. The RTS is mounted on the main tower crossbeam, and the controllable points (i.e., benchmark) for both the CPS and the proposed CNS is also the main tower. In addition, the comparison in this paper is the deflection change. In other words, the initial values are chosen first, and then the change in deflections relative to the initial values are compared.

First, as the common deflection measurement method for large-span bridge, the RTS was adopted herein to provide the reference value of bridge deflection. In this experiment, the RTS used was Leica TS-60, and the regular prism is selected as the measuring point. As shown in Figure 8a, the RTS is fixed on the crossbeam of the main tower to ensure a stable platform. By switching the RTS to the automatic tracking measurement mode, automatic monitoring was conducted with a frequency of 1 Hz. Note that the RTS cannot simultaneously measure multiple points for large-span bridges. Hence, the deflections at 1/16 span and 1/4 span of bridge were successively monitored for 6 h (from 8:00 a.m. to 14:00 p.m. on July 31, 2021) and 4 h (from 11:00 a.m. to 15:00 p.m. on July 30, 2021), respectively. Figure 9 compares the deflection change based on the RTS, CNS, and CV methods. The deflections observed with CNS are generally consistent with those obtained using RTS, while it is difficult to accurately obtain the deflection change of the bridge with CV method without the motion compensation. Both the RTS and CNS can capture the dynamic response of the bridge

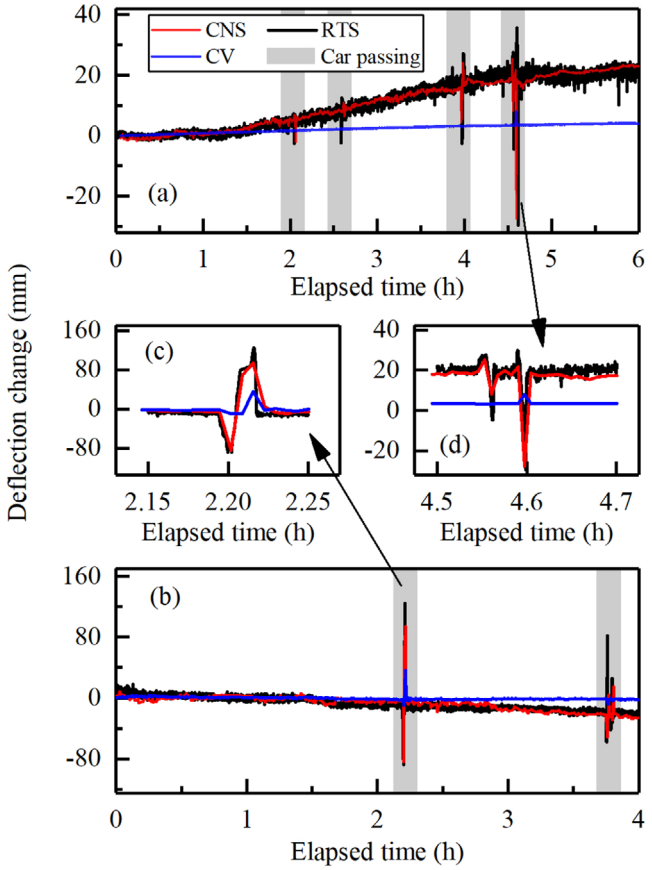

FIGURE 9 Comparison of the measured bridge deflections based on robotic total station (RTS), camera network system (CNS), and traditional computer vision (CV): (a) 1/16 span, (b) 1/4 span, (c) enlarged view of the 1/4 span deflection response during one vehicle passage, (d) enlarged view of the 1/16 span deflection response during two vehicles passage.

TABLE 3 Measurement difference compared with robotic total station (RTS).

Measurement difference	CNS		CV	
	1/16 span	1/4 span	1/16 span	1/4 span
Mean value (mm)	0.29	0.30	9.36	8.79
Root mean square value (mm)	1.28	3.31	11.81	13.08

due to vehicle load. When the vehicle passed, the observed peak values of bridge deflection based on RTS and CNS are different (Figure 9c,d), which is mainly due to the difference of measuring frequency and the asynchronism of those two methods. Hence, the measurement errors of this experiment are calculated by excluding the vehicle-induced deflection. As shown in Table 3, compared with RTS, the root mean square values of measurement difference based on the proposed CNS are lower than 3.4 mm, which reveal the feasibility and stability of the long-term monitoring of CNS.

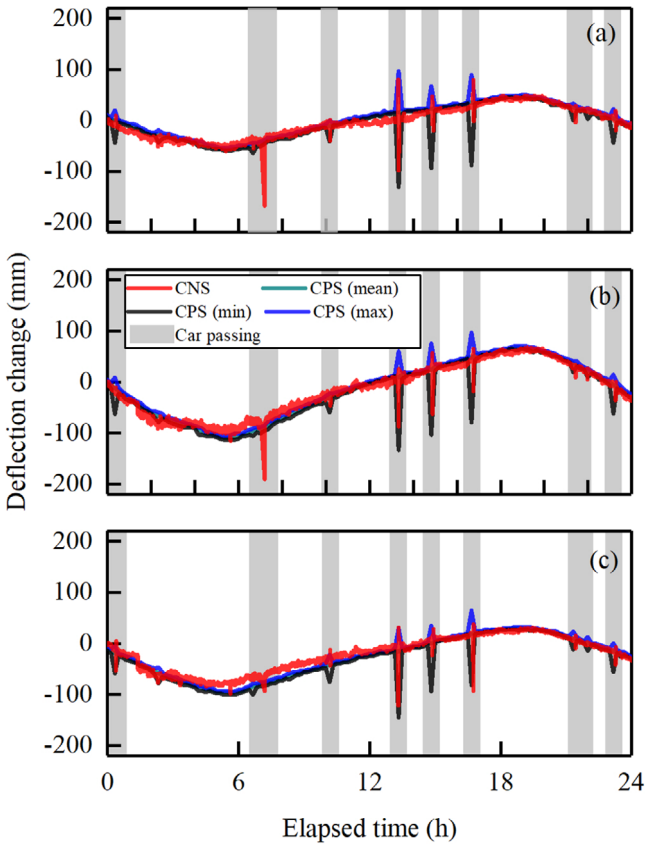

FIGURE 10 Comparison of the measured bridge deflections based on connected pipe system (CPS) and camera network system (CNS): (a) 1/4, (b) 1/2, and (c) 3/4 span.

Furthermore, the proposed CNS was compared with the existing CPS in the studied bridge. As shown in Figure 8c, the CPS was arranged in the steel box girder using the pressure transmitters at 1/16 span intervals. It is worth noting that only the maximum, minimum, and mean values of deflection were given through the CPS in a period of 10 min since the bridge was not yet in operation. From 00:00 to 24:00 on August 1, 2021, the results of monitoring the 24-h deflection change based on CPS and CNS are compared herein. As depicted in Figure 10, at a different span of the suspension bridge, the observed bridge deflection with CPS and CNS are consistent in trend and are similar in value, which reveals the stability of the proposed CNS system.

4 | OBSERVED FULL-SPAN DEFLECTION OF SUSPENSION BRIDGE

Compared with the traditional CPS, the number of measurement points is ideally unlimited by simply adding the prisms in the proposed CNS system. In this case, the deflection of 43 points (10 camera stations and 33

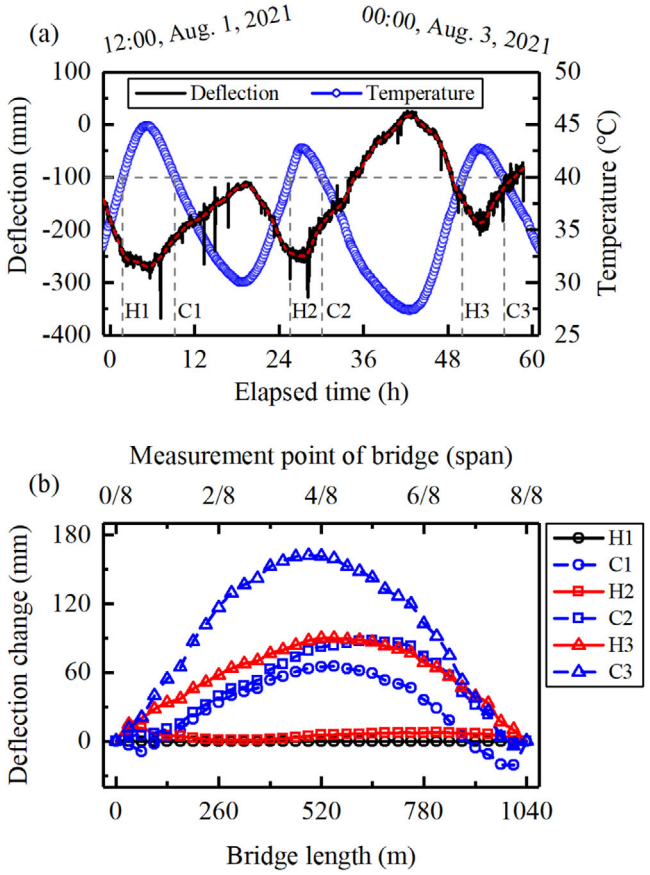

FIGURE 11 Evolution of deflection and temperature with elapsed time: (a) deflection versus temperature at 1/2 span, (b) full-span deflection at a same temperature of 40°C.

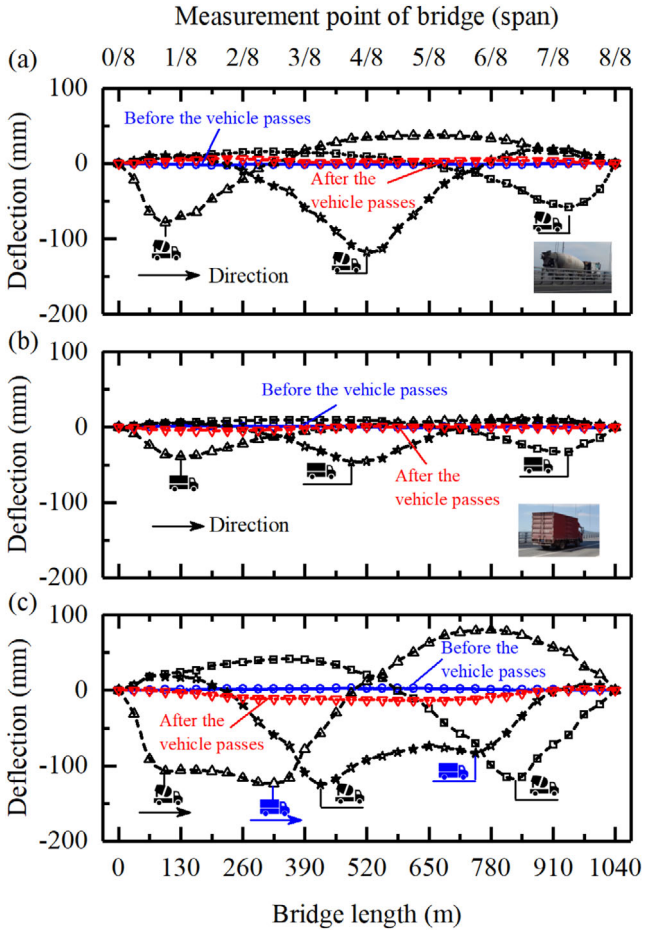

FIGURE 12 Effect of vehicle load on the full-span deflection evolution of bridge: (a) heavy truck, (b) medium truck, and (c) heavy and medium truck.

prisms) can simultaneously be measured along the bridge. Thus, the geometric alignment of the bridge with dense multimeasuring points can be obtained, which can better parameters for the response analysis of suspension bridge. Figure 11 depicts both the evolution of deflection and temperature with elapsed time at 1/2 span of bridge. In the long term, the trend of bridge deflection is dominated by the temperature and well correlated with the temperature change. For the studied suspension bridge, the downward deflection can be observed during the heating process, while cooling typically leads to the upward deflection. As shown in Figure 11a, the minimum and maximum temperature during the 60-h monitoring are 27.4°C and 44.9°C, respectively, corresponding to the maximum and minimum deflection of about 20 mm and −270 mm, respectively. To further investigate the relationship between bridge deflection response and temperature loading, the full-span bridge deflection at the temperature 40°C (i.e., H1, C1, H2, C2, H3, C3 in Figure 11a) are presented and compared. Figure 11b depicts the relative deflection compared to the deflection at the time of H1. It can be seen that the bridge deflections differ a lot although the corresponding temperatures are the same (40°C). Specifically, during the hearing process, the bridge deflections at the time of H1 and H2 are similar, which are quite different from the observed value at the time of H3. This is mainly because there is little difference between the peak temperature in the heating stage at time H1 and H2, while a significant decrease of the minimum temperature can be observed during the heating stage of H3. Hence, it can be concluded that the bridge deflection varies periodically with temperature, whereas the deflection is not linearly correlated with the temperature. The long-term geometric line of the suspension bridge is affected by many factors, including but not limited to the initial temperature and temperature change.

In a short time, the bridge deflection is mainly affected by the vehicle and wind load. To further discuss the effect of vehicle load on the bridge deflection evolution, Figure 12 depicts the full-span relative deflection compared with the deflection before the vehicle passed. A sine-like wave of bridge deflection can be observed due to vehicle load. The vehicle typically leads to a most downward deflection

at its location of bridge, which decreases with the distance to the vehicle and even an upward deflection. After the vehicle passed, the bridge deflection recovers rapidly, which is almost consistent with that before. In addition, the vehicle-induced magnitude of the bridge deflection is directly determined by the number and load of vehicle. As shown in Figure 12a, the value of relative deflections when the concrete mixer truck passed 1/8, ¼, and 7/8 span of the bridge are −78.3 mm, −118.5 mm, and −57.8, respectively. Similarly, when the van pass, as shown in Figure 12b, the relative deflections at 1/8, ¼, and 7/8 span are reduced to −38.8 mm, −46.4 mm, and −33.5 mm, respectively. Under the combined effect of concrete mixer truck and van, the magnitude of the bridge deflection is much larger, as shown in Figure 12c. In addition, it can be observed that the passing position of the vehicles are the knee points of the bridge geometric line type, which can be used for the reverse calculation of vehicle position and load.

5 | DISCUSSION

The proposed CNS was demonstrated to be a feasible and effective measurement means. However, to adapt to different bridge engineering site environments, there are still some challenges that remain to be further investigated, including but not limited to the following:

1. Optimal design of CNS: Using denser cameras or upgrading the resolution of cameras can continue to increase the spatial resolution. It is worth noting that the design of the number of cameras in the monitoring system is a multiobjective optimization problem, which needs to consider a variety of parameters, such as measurement accuracy, cost, and robustness.
2. Field implementation: The CNS in this study was established in the steel box girder of the bridge, which is a main feature and advantage of the proposed system. This is mainly because the steel box girder has a relatively closed and simple monitoring environment. When CNS is arranged outdoors, special attention should be paid to the effect of optical turbulence (Luo et al., 2020), the condensation of water droplets on the lens caused by temperature change (Shajihan et al., 2022), and the interference of rain, snow, and fog on the visual measurement.
3. Data postprocessing: Based on the measured geometric alignment of the bridge, a preliminary analysis on the effect of temperature and vehicle load has been conducted herein. A further data mining and analysis are necessary. In addition, combining the proposed CNS with the latest advances in machine learning techniques is an ongoing research effort (Amezquita-Sanchez et al., 2018).

6 | CONCLUSIONS

A bridge deflection vision monitoring method that can well compensate the camera motion–induced errors is proposed in this study. By arranging the dual-head camera station and cooperative marker along the bridge, the CNS can be established to obtain the multipoint deflection of a large-span bridge. By integrating an infrared illumination supplement device in the camera station and cooperating with the regular double-sided prism (i.e., cooperative marker), the 24-h continuous monitoring can be realized.

The feasibility and efficiency of the proposed CNS are verified through the field test of a suspension bridge. The quasi-static validation results show that the proposed CNS can effectively compensate the motion-induced error of the camera station and achieve submillimeter measurement accuracy. For the long-term monitoring, the bridge deflections observed by CNS agree well with those obtained using the existing RTS and CPS.

The effect of operating load on the observed bridge deflection is further discussed. A sine-like wave evolution of bridge deflection can be observed through the proposed CNS due to vehicle load. In the long term, the bridge deflection is correlated with the temperature change. The efficiency and stability of the related algorithm remain to be studied.

ACKNOWLEDGMENTS

This work was supported by the National Key Research and Development Program of China (No. 2019YFC1511102), the National Natural Science Foundation of China (No. 12002215 & No. 52208399), and the China Postdoctoral Science Foundation (No. 2021M702266 & No. 2022T150437).

REFERENCES

Adeli, H., & Saleh, A. (1997). Optimal control of adaptive/smart bridge structures. *Journal of Structural Engineering*, *123*(2), 218–226. https://doi.org/10.1061/(ASCE)0733-9445(1997)123:2(218)

Amezquita-Sanchez, J. P., & Adeli, H. (2019). Nonlinear measurements for feature extraction in structural health monitoring. *Scientia Iranica*, *26*(6), 3051–3059. https://doi.org/10.24200/sci.2019.21669

Amezquita-Sanchez, J. P., Park, H. S., & Adeli, H. (2017). A novel methodology for modal parameters identification of large smart structures using MUSIC, empirical wavelet transform, and Hilbert transform. *Engineering Structures*, *147*, 148–159. https://doi.org/10.1016/j.engstruct.2017.05.054

Amezquita-Sanchez, J. P., Valtierra-Rodriguez, M., & Adeli, H. (2018). Wireless smart sensors for monitoring the health condition of civil infrastructure. *Scientia Iranica*, *25*(6), 2913–2925.

Bao, Y., Chen, Z., Wei, S., Xu, Y., Tang, Z., & Li, H. (2019). The state of the art of data science and engineering in structural health monitoring. *Engineering*, *5*(2), 234–242. https://doi.org/10.1016/j.eng.2018.11.027

Chen, I.-H., Ho, S.-C., & Su, M.-B. (2020). Computer vision application programming for settlement monitoring in a drainage tunnel. *Automation in Construction*, *110*, 103011. https://doi.org/10.1016/j.autcon.2019.103011

Chun, P.-J., Yamane, T., & Maemura, Y. (2022). A deep learning-based image captioning method to automatically generate comprehensive explanations of bridge damage. *Computer-Aided Civil and Infrastructure Engineering*, *37*(11), 1387–1401. https://doi.org/10.1111/mice.12793

Dong, C.-Z., & Catbas, F. N. (2021). A review of computer vision–based structural health monitoring at local and global levels. *Structural Health Monitoring*, *20*(2), 692–743.

Dos Santos, R. C., Larocca, A. P. C., de Araújo Neto, J. O., Barbosa, A. C. B., & Oliveira, J. V. M. (2019). Detection of a curved bridge deck vibration using robotic total stations for structural health monitoring. *Journal of Civil Structural Health Monitoring*, *9*(1), 63–76. https://doi.org/10.1007/s13349-019-00322-1

Feng, D., & Feng, M. Q. (2018). Computer vision for SHM of civil infrastructure: From dynamic response measurement to damage detection—A review. *Engineering Structures*, *156*, 105–117. https://doi.org/10.1016/j.engstruct.2017.11.018

Feng, D., Feng, M. Q., Ozer, E., & Fukuda, Y. (2015). A vision-based sensor for noncontact structural displacement measurement. *Sensors*, *15*(7), 16557–16575. Article 7. https://doi.org/10.3390/s150716557

Ghaedi, K., Ibrahim, Z., Adeli, H., & Javanmardi, A. (2017). Invited review: Recent developments in vibration control of building and bridge structures. *Journal of Vibroengineering*, *19*(5), 3564–3580. Article 5. https://doi.org/10.21595/jve.2017.18900

Gutierrez Soto, M., & Adeli, H. (2019). Semi-active vibration control of smart isolated highway bridge structures using replicator dynamics. *Engineering Structures*, *186*, 536–552. https://doi.org/10.1016/j.engstruct.2019.02.031

Hampshire, T. A., & Adeli, H. (2000). Monitoring the behavior of steel structures using distributed optical fiber sensors. *Journal of Constructional Steel Research*, *53*(3), 267–281. https://doi.org/10.1016/S0143-974X(99)00043-7

Kim, H., & Adeli, H. (2005). Wavelet-hybrid feedback linear mean squared algorithm for robust control of cable-stayed bridges. *Journal of Bridge Engineering*, *10*(2), 116–123. https://doi.org/10.1061/(ASCE)1084-0702(2005)10:2(116)

Lee, H. M., & Park, H. S. (2011). Gage-free stress estimation of a beam-like structure based on terrestrial laser scanning. *Computer-Aided Civil and Infrastructure Engineering*, *26*(8), 647–658. https://doi.org/10.1111/j.1467-8667.2011.00723.x

Lee, J., Lee, K.-C., Jeong, S., Lee, Y.-J., & Sim, S.-H. (2020). Long-term displacement measurement of full-scale bridges using camera ego-motion compensation. *Mechanical Systems and Signal Processing*, *140*, 106651. https://doi.org/10.1016/j.ymssp.2020.106651

Li, H., Ou, J., Zhang, X., Pei, M., & Li, N. (2015). Research and practice of health monitoring for long-span bridges in the Mainland of China. *Smart Structures and Systems*, *15*(3), 555–576. https://doi.org/10.12989/sss.2015.15.3.555

Li, H., Ou, J., Zhao, X., Zhou, W., Li, H., Zhou, Z., & Yang, Y. (2006). Structural health monitoring system for the Shandong Binzhou Yellow River highway bridge. *Computer-Aided Civil and Infrastructure Engineering*, *21*(4), 306–317.

Liu, Y., Deng, Y., & Cai, C. S. (2015). Deflection monitoring and assessment for a suspension bridge using a connected pipe system: A case study in China. *Structural Control and Health Monitoring*, *22*(12), 1408–1425. https://doi.org/10.1002/stc.1751

Luo, L., Feng, M. Q., & Wu, J. (2020). A comprehensive alleviation technique for optical-turbulence-induced errors in vision-based displacement measurement. *Structural Control and Health Monitoring*, *27*(3), e2496. https://doi.org/10.1002/stc.2496

Lydon, D., Lydon, M., Taylor, S., Del Rincon, J. M., Hester, D., & Brownjohn, J. (2019). Development and field testing of a vision-based displacement system using a low cost wireless action camera. *Mechanical Systems and Signal Processing*, *121*, 343–358. https://doi.org/10.1016/j.ymssp.2018.11.015

Nasimi, R., & Moreu, F. (2021). A methodology for measuring the total displacements of structures using a laser–camera system. *Computer-Aided Civil and Infrastructure Engineering*, *36*(4), 421–437. https://doi.org/10.1111/mice.12652

Ngeljaratan, L., Moustafa, M. A., & Pekcan, G. (2021). A compressive sensing method for processing and improving vision-based target-tracking signals for structural health monitoring. *Computer-Aided Civil and Infrastructure Engineering*, *36*(9), 1203–1223. https://doi.org/10.1111/mice.12653

Niu, Y., Ye, Y., Zhao, W., & Shu, J. (2021). Dynamic monitoring and data analysis of a long-span arch bridge based on high-rate GNSS-RTK measurement combining CF-CEEMD method. *Journal of Civil Structural Health Monitoring*, *11*(1), 35–48. https://doi.org/10.1007/s13349-020-00436-x

Oh, B. K., Kim, K. J., Kim, Y., Park, H. S., & Adeli, H. (2017). Evolutionary learning based sustainable strain sensing model for structural health monitoring of high-rise buildings. *Applied Soft Computing*, *58*, 576–585.

Pan, B., Tian, L., & Song, X. (2016). Real-time, non-contact and targetless measurement of vertical deflection of bridges using off-axis digital image correlation. *NDT & E International*, *79*, 73–80. https://doi.org/10.1016/j.ndteint.2015.12.006

Park, H. S., Lee, H. M., Adeli, H., & Lee, I. (2007). A new approach for health monitoring of structures: Terrestrial laser scanning. *Computer-Aided Civil and Infrastructure Engineering*, *22*(1), 19–30. https://doi.org/10.1111/j.1467-8667.2006.00466.x

Park, S. W., Park, H. S., Kim, J. H., & Adeli, H. (2015). 3D displacement measurement model for health monitoring of structures using a motion capture system. *Measurement*, *59*, 352–362. https://doi.org/10.1016/j.measurement.2014.09.063

Perez-Ramirez, C. A., Amezquita-Sanchez, J. P., Adeli, H., Valtierra-Rodriguez, M., Camarena-Martinez, D., & Romero-Troncoso, R. J. (2016). New methodology for modal parameters identification of smart civil structures using ambient vibrations and synchrosqueezed wavelet transform. *Engineering Applications of Artificial Intelligence*, *48*, 1–12. https://doi.org/10.1016/j.engappai.2015.10.005

Perez-Ramirez, C. A., Amezquita-Sanchez, J. P., Valtierra-Rodriguez, M., Adeli, H., Dominguez-Gonzalez, A., & Romero-Troncoso, R. J. (2019). Recurrent neural network model with Bayesian training and mutual information for response prediction of large buildings. *Engineering Structures*, *178*, 603–615. https://doi.org/10.1016/j.engstruct.2018.10.065

Pezeshki, H., Pavlou, D., Adeli, H., & Siriwardane, S. C. (2023). Modal analysis of offshore wind turbine structures: An analytical solution, *ASME Journal of Offshore Mechanics and Arctic Engineering*, *145*(1), 010907. (18 pages).

Psimoulis, P. A., & Stiros, S. C. (2013). Measuring deflections of a short-span railway bridge using a robotic total station. *Journal of Bridge Engineering*, *18*(2), 182–185. https://doi.org/10.1061/(ASCE)BE.1943-5592.0000334

Ren, Q., Li, M., Li, H., Song, L., Si, W., & Liu, H. (2021). A robust prediction model for displacement of concrete dams subjected to irregular water-level fluctuations. *Computer-Aided Civil and Infrastructure Engineering*, *36*(5), 577–601. https://doi.org/10.1111/mice.12654

Sajedi, S. O., & Liang, X. (2021). Uncertainty-assisted deep vision structural health monitoring. *Computer-Aided Civil and Infrastructure Engineering*, *36*(2), 126–142. https://doi.org/10.1111/mice.12580

Shajihan, S. A. V., Hoang, T., Mechitov, K., & Spencer, B. F. Jr. (2022). Wireless SmartVision system for synchronized displacement monitoring of railroad bridges. *Computer-Aided Civil and Infrastructure Engineering*, *37*(9), 1070–1088. https://doi.org/10.1111/mice.12846

Shang, Y., Yu, Q., Yang, Z., Xu, Z., & Zhang, X. (2014). Displacement and deformation measurement for large structures by camera network. *Optics and Lasers in Engineering*, *54*, 247–254. https://doi.org/10.1016/j.optlaseng.2013.07.009

Sirca, G. F. Jr., & Adeli, H. (2018). Infrared thermography for detecting defects in concrete structures. *Journal of Civil Engineering and Management*, *24*(7), 508–515. Article 7. https://doi.org/10.3846/jcem.2018.6186

Sousa Tomé, E., Pimentel, M., & Figueiras, J. (2020). Damage detection under environmental and operational effects using cointegration analysis—Application to experimental data from a cable-stayed bridge. *Mechanical Systems and Signal Processing*, *135*, 106386. https://doi.org/10.1016/j.ymssp.2019.106386

Spencer, B. F., Hoskere, V., & Narazaki, Y. (2019). Advances in computer vision-based civil infrastructure inspection and monitoring. *Engineering*, *5*(2), 199–222.

Stephen, G. A., Brownjohn, J. M. W., & Taylor, C. A. (1993). Measurements of static and dynamic displacement from visual monitoring of the Humber Bridge. *Engineering Structures*, *15*(3), 197–208. https://doi.org/10.1016/0141-0296(93)90054-8

Tian, Y., Zhang, C., Jiang, S., Zhang, J., & Duan, W. (2021). Noncontact cable force estimation with unmanned aerial vehicle and computer vision. *Computer-Aided Civil and Infrastructure Engineering*, *36*(1), 73–88. https://doi.org/10.1111/mice.12567

Wang, G., Shi, Z., Shang, Y., & Yu, Q. (2018). Automatic extraction of diagonal markers based on template matching and peaks of gradient histogram. *Acta Optica Sinica*, *38*(8), 0815014. https://doi.org/10.3788/AOS201838.0815014

Yi, T.-H., Li, H.-N., & Gu, M. (2013). Recent research and applications of GPS-based monitoring technology for high-rise structures. *Structural Control & Health Monitoring*, *20*(5), 649–670. https://doi.org/10.1002/stc.1501

Yu, J., Meng, X., Shao, X., Yan, B., & Yang, L. (2014). Identification of dynamic displacements and modal frequencies of a medium-span suspension bridge using multimode GNSS processing. *Engineering Structures*, *81*, 432–443. https://doi.org/10.1016/j.engstruct.2014.10.010

Yu, Q., Guan, B., Shang, Y., Liu, X., & Li, Z. (2019). Flexible camera series network for deformation measurement of large scale structures. *Smart Structures and Systems*, *24*(5), 587–595. https://doi.org/10.12989/sss.2019.24.5.587

Yu, Q., Jiang, G., Shang, Y., Xu, Y., Liu, X., Fu, S., Guan, B., & Zhu, X. (2015). A displacement-relay videometric method for surface subsidence surveillance in unstable areas. *Science China Technological Sciences*, *58*(6), 1105–1111. https://doi.org/10.1007/s11431-015-5811-6

Yu, Q., Yin, Y., Zhang, Y., Chen, W., Hu, B., & Liu, X. (2022). Displacement measurement of large structures using nonoverlapping field of view multi-camera systems under six degrees of freedom egomotion. *Computer-Aided Civil and Infrastructure Engineering*, *00*, 1–21. https://doi.org/10.1111/mice.12966

Yu, S., & Zhang, J. (2020). Fast bridge deflection monitoring through an improved feature tracing algorithm. *Computer-Aided Civil and Infrastructure Engineering*, *35*(3), 292–302. https://doi.org/10.1111/mice.12499

Zhang, J., Zhou, L., Tian, Y., Yu, S., Zhao, W., & Cheng, Y. (2021). Vortex-induced vibration measurement of a long-span suspension bridge through noncontact sensing strategies. *Computer-Aided Civil and Infrastructure Engineering*, *37*(12), 1617–1633. Advance online publication. https://doi.org/10.1111/mice.12712

Zhang, Y., & Lin, W. (2022). Computer-vision-based differential remeshing for updating the geometry of finite element model. *Computer-Aided Civil and Infrastructure Engineering*, *37*(2), 185–203. https://doi.org/10.1111/mice.12708

Zhao, J., Bao, Y., Guan, Z., Zuo, W., Li, J., & Li, H. (2019). Video-based multiscale identification approach for tower vibration of a cable-stayed bridge model under earthquake ground motions. *Structural Control and Health Monitoring*, *26*(3), e2314. https://doi.org/10.1002/stc.2314

Zhao, J., Hu, F., Xu, Y., Zuo, W., Zhong, J., & Li, H. (2022). StructurePoseNet for identification of dense dynamic displacement and three-dimensional poses of structures using a monocular camera. *Computer-Aided Civil and Infrastructure Engineering*, *37*(6), 704–725. https://doi.org/10.1111/mice.12761

Zheng, Y., Gao, Y., Lu, S., & Mosalam, K. M. (2022). Multistage semisupervised active learning framework for crack identification, segmentation, and measurement of bridges. *Computer-Aided Civil and Infrastructure Engineering*, *37*(9), 1089–1108. https://doi.org/10.1111/mice.12851

Zhou, J., Sun, Z., Wei, B., Zhang, L., & Zeng, P. (2021). Deflection-based multilevel structural condition assessment of long-span prestressed concrete girder bridges using a connected pipe system. *Measurement*, *169*, 108352. https://doi.org/10.1016/j.measurement.2020.108352

Zhuge, S., Xu, X., Zhong, L., Gan, S., Lin, B., Yang, X., & Zhang, X. (2022). Noncontact deflection measurement for bridge through a multi-UAVs system. *Computer-Aided Civil and Infrastructure Engineering*, *37*(6), 746–761. https://doi.org/10.1111/mice.12771

How to cite this article: Yin, Y., Yu, Q., Hu, B., Zhang, Y., Chen, W., Liu, X., & Ding, X. (2023). A vision monitoring system for multipoint deflection of large-span bridge based on camera networking. *Computer-Aided Civil and Infrastructure Engineering*, *38,* 1879–1891. https://doi.org/10.1111/mice.13050